Panchromatic Sensitization Using Zn(II) Porphyrin-Based Photosensitizers for Light-Driven Hydrogen Production in Water

Po-Yu Ho[†],[a] Michael F. Mark[†],[b] Yi Wang,[a] Sze-Chun Yiu,[a] Wai-Hong Yu,[a] Cheuk-Lam Ho,*[a] David W. McCamant,*[b] Richard Eisenberg,[b] and Shuping Huang*[c]

[a] *Dr. P.-Y. Ho,[†] Y. Wang, Dr. S.-C. Yiu, W.-H. Yu, Dr. C.-L. Ho*

Department of Applied Biology and Chemical Technology

The Hong Kong Polytechnic University

Hong Hom, Hong Kong (P.R. China)

E-mail: cheuk-lam.ho@polyu.edu.hk

[b] *M. F. Mark,[†] Dr. D. W. McCamant, Prof. R. Eisenberg*

Department of Chemistry

University of Rochester

Rochester, New York 14627 (United States)

E-mail: mccamant@chem.rochester.edu

[c] *Dr. S. Huang*

College of Chemistry

Fuzhou University

Fuzhou, Fujian 350108 (P.R. China)

E-mail: huangshp@gmail.com

[†] *These authors contributed equally to this work.*

ABSTRACT: Three molecular photosensitizers (PSs) with carboxylic acid anchors for attachment to platinized titanium dioxide nanoparticles were studied for light-driven hydrogen production from a fully aqueous medium with ascorbic acid (AA) as the sacrificial electron donor. Two zinc(II) porphyrin (ZnP) based PSs (**ZnP-dyad** and **YD2-o-C8**) were used to examine the effect of panchromatic sensitization in promoting photocatalytic H_2 generation. A dyad molecular design was used to construct the Bodipy-conjugated ZnP PS (**ZnP-dyad**) and another one was featured with an electron-donating diarylamino moiety (**YD2-o-C8**). In order to probe the good use of the ZnP scaffold in this particular energy conversion process, an organic PS without the ZnP moiety (**Bodipy-dye**) was also synthesized for comparison. Ultrafast transient absorption spectroscopy was adopted to map out the energy transfer processes occurring in the dyad and establish the Bodipy-based antenna effect. In particular, the systems with **YD2-o-C8** and **ZnP-dyad** achieve a remarkable initial activity in H_2 production with an initial turnover frequency (TOF_i) larger than 300 h^{-1} under white light irradiation. In brief, the use of ZnP PSs in dye-sensitized photocatalysis for H_2 evolution reaction in this study indicates the importance of panchromatic sensitization capability for the development of light absorbing PSs.

Introduction

Energy is probably one of the most critical factors that will shape our society in the 21st century.[1] Scientists and engineers are making efforts to expand the dimensions of energy resources, because excessive burning of fossil fuel will bring about local air pollution problems and global climate change.[2] Harnessing solar energy to produce hydrogen fuel from water through a water splitting reaction represents one of the prospective ways to support sustainable development and exploit alternative energy resources.[3] Hydrogen is considered as an ideal energy carrier with no carbon footprint and can be generated from water, with a tremendous amount of feed-stock freely provided by mother nature.[4] In addition, H_2 fuel can be further utilized as a reagent to produce other important industrial chemicals, such as methane and methanol.[5]

In regards to water splitting reaction, this key energy-storing reaction can be comprehended as two redox half reactions: i) reduction of two aqueous protons to one H_2 at the cathodic side and ii) oxidation of two water molecules to one O_2 molecule at the anodic side.[6] In this study, we focus on the reductive side of water splitting, concentrating on efforts dealing with photocatalytic H_2 generation based on the simplest form, which demands a photosensitizer (PS) for exciton formation, a pathway for charge separation, a catalyst converting two aqueous protons into a hydrogen molecule, and a source of electrons (i.e. sacrificial electron donor).[7]

In the past few decades, metal complex-based PSs that absorb visible light have been broadly investigated for water reduction. In particular, most of these PSs are comprised of noble metals, such as ruthenium(II), iridium(III) and platinum(II) metal centers.[7-8] However, these charge transfer complexes typically suffer from inefficient photon capture because of their poor absorption in the blue−green region of the spectrum and low molar absorptivities (~ 7–15 × 10^3

M^{-1} cm^{-1}).[9] In 2015, Zheng et al. reported new dyads consisting of a strongly absorbing Bodipy (dipyrromethene-BF_2) and a platinum diimine dithiolate (PtN_2S_2) chromophore, which, when grafted onto platinized TiO_2 nanoparticles (TiO_2-Pt), showed much greater efficiency in harvesting photons at 530 nm than the PtN_2S_2 chromophores alone.[10] Therefore, this dyad approach improves upon the aforementioned drawbacks for the noble metal charge transfer complexes.

Along this direction, it is of great interest to find or develop a new category of noble metal-free dyes with strong and panchromatic sensitization property for H_2 generation. In nature, porphyrin and its derivatives are the chromophores adopted as the solar photosynthetic cores in plants and bacteria.[11] In general, free-base and metallated porphyrin absorption spectra are characterized by strong Soret-band(s) absorbing blue light ($\varepsilon > 10^5$ M^{-1} cm^{-1} around 400 nm) and Q-bands centered between 500–700 nm ($\varepsilon > 10^4$ M^{-1} cm^{-1}).[12] Due to this attractive dual-absorption band feature, ZnP derivatives have been extensively investigated for dye-sensitized solar cells (DSSCs) for the last decade.[11a] In this area, Yeh et al. made a great contribution in optimizing ZnP-based dyes, whereas they found the electronic push-pull effect gave large impacts towards the power conversion efficiency (PCE).[13] In 2011 to 2012, alkoxy-wrapped push-pull ZnP dyes were reported to achieve PCEs > 8% in the corresponding DSSCs, and the long alkoxy chains in the *ortho*-positions of the *meso*-phenyl groups on the porphyrin scaffold were found to reduce dye aggregation and boost the charge collection yield.[14] Nevertheless, studies exploiting molecular engineered ZnP PSs for light-driven hydrogen production based on PS-TiO_2-Pt hybrid material remain scarce.

In 2010, Lee and Hupp synthesized a new molecular dyad containing a Bodipy organic chromophore covalently linked through a phenyl-ethynyl linkage to ZnP, which showed

increased photon-to-current conversion efficiency in a dye-sensitized solar cell (DSSC).[15] While this chromophore showed improved DSSC efficiency, it has not yet been utilized as a PS for hydrogen production, nor has the ultrafast dynamics associated with the energy transfer events in the dyad been characterized. In this work, we utilize a similar molecular dyad, **ZnP-dyad,** containing small changes in the aliphatic tails, as a solar hydrogen production PS and we fully characterize the Bodipy to ZnP energy transfer dynamics.

Herein, we describe a light-driven hydrogen production study utilizing three different anchor-containing PSs (Figure 1) and the corresponding PS-TiO_2-Pt composite materials. One of the PSs **YD2-o-C8** (a highly efficient ZnP dye for DSSCs firstly reported in 2011[14a, 14b]) is systematically compared with the designated Bodipy-conjugated ZnP dye (**ZnP-dyad**). Ultrafast transient absorption spectroscopy is used to study the energy transfer processes initiated from different excited states of **ZnP-dyad** (shown in Scheme 1). Also, an organic PS featuring a Bodipy unit (**Bodipy-dye**) is synthesized to compare and contrast the light-harvesting effects attributed by the ZnP unit. In addition, since **ZnP-dyad** and **YD2-o-C8** are both panchromatic in nature, both green and white lights are used to examine the significance brought from the panchromatic sensitization as well as the effect(s) given by the dyad molecular design. The results reveal a number of factors that should be considered in designing an ideal molecular PS for light-driven hydrogen generation from aqueous media.

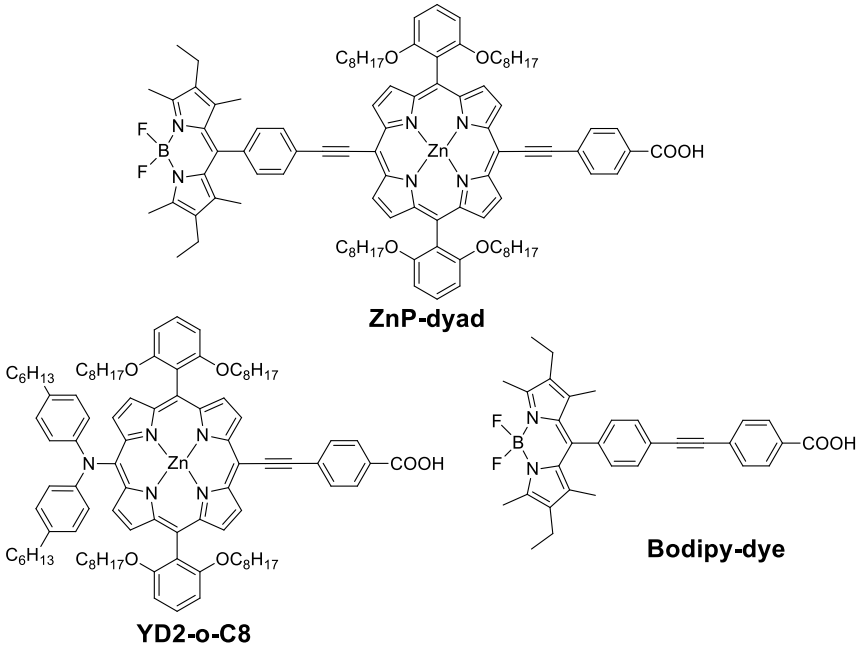

Figure 1. Chemical structures of PSs **ZnP-dyad**, **YD2-o-C8** and **Bodipy-dye**.

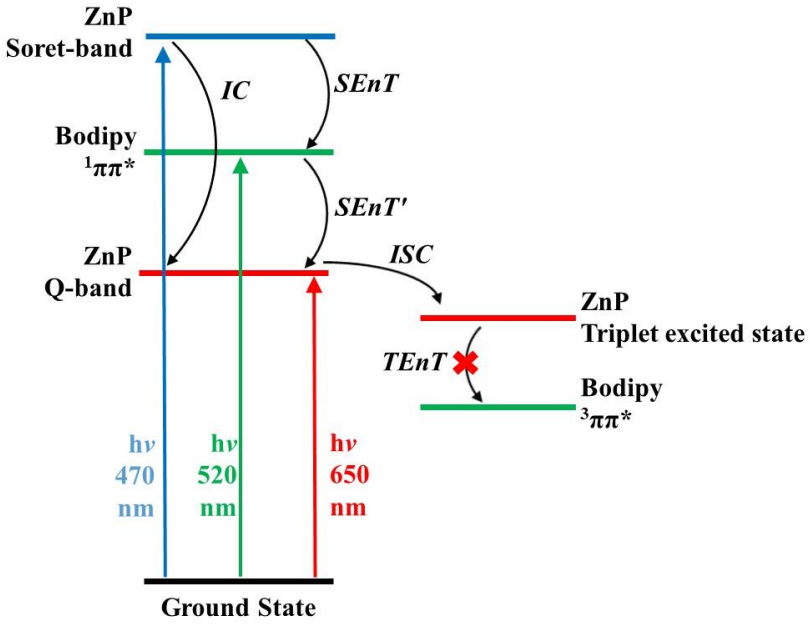

Scheme 1. Possible processes involved upon excitation of **ZnP-dyad** (SEnT = singlet energy transfer, IC = internal conversion, ISC = intersystem crossing, and TEnT = triplet energy transfer).

Results and Discussion

Synthesis and characterization

The synthetic routes of **ZnP-dyad** and **Bodipy-dye** are shown in Scheme 2 and the detailed procedures are shown in Experimental section. The key intermediates, iodo-compound (**1**) and **ZnP** (i.e. TIPS-protected diethynyl Zn(II) porphyrin moiety) were synthesized according to the reported procedures.[15-16] For the pure organic molecule **Bodipy-dye**, it was prepared by Sonogashira coupling with 4-iodobenzoic acid (ca. 80% yield) after embedding an ethynyl group on compound **1**. For the Bodipy-conjugated ZnP dyad, deprotection at the ethynyl groups using tetra-*n*-butylammonium fluoride and further unsymmetrical Sonogashira coupling with 4-iodobenzoic acid and compound **1** rendered the corresponding product **ZnP-dyad** in ca. 50% yield. All the intermediates and target compounds were purified by column chromatography on silica gel, and fully characterized by ^{1}H and ^{13}C spectroscopies and matrix-assisted laser desorption ionization time-of-flight (MALDI-TOF) mass spectrometry.

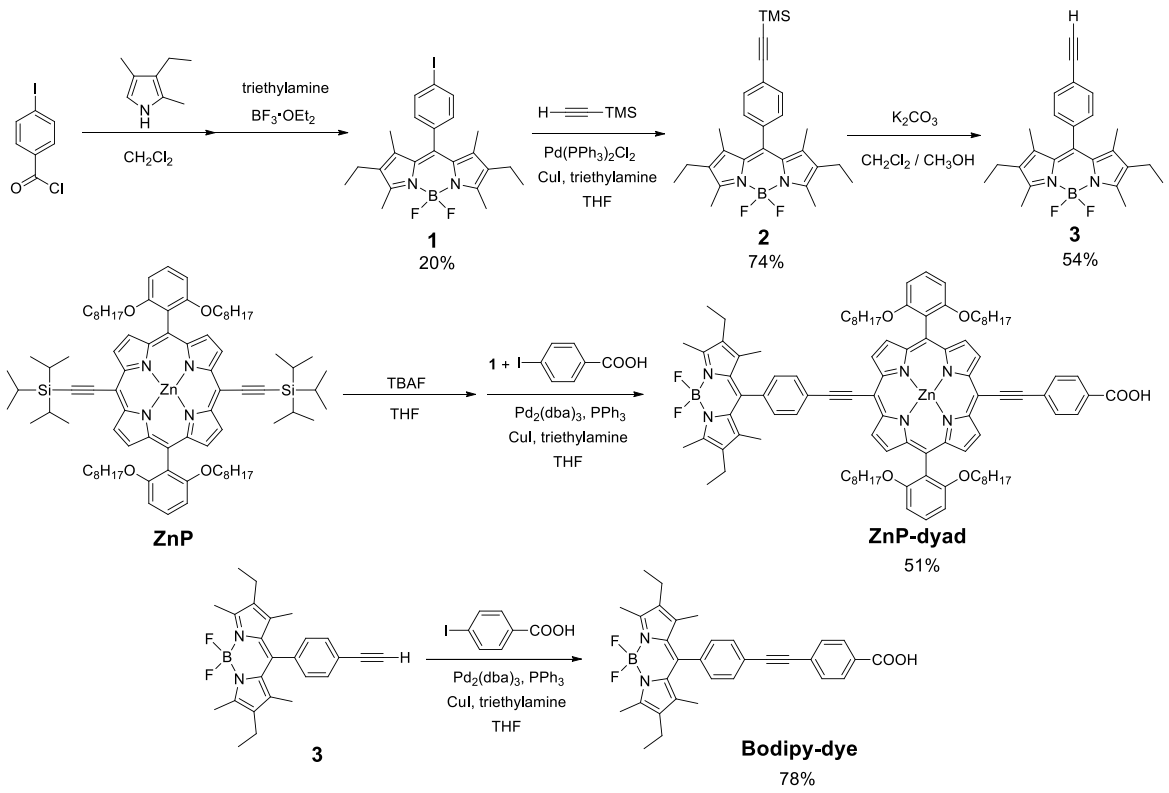

Scheme 2. Synthetic routes for **ZnP-dyad** and **Bodipy-dye**.

Photophysical properties

The photophysical properties of **ZnP-dyad**, **YD2-o-C8** and **Bodipy-dye** were studied in CH_2Cl_2 solutions at ambient temperature. Their UV-vis absorption spectra and emission spectra are shown in Figures 2 and S11, respectively, and the corresponding data are tabulated in Table 1. For the organic PS **Bodipy-dye**, it resembles the characteristics of typical Bodipy chromophores in both absorption and fluorescence spectra. A sharp band at 526 nm is observed in the absorption spectrum and an emission peak is observed at 544 nm, both due to the S_0–S_1 ($^1\pi\pi^*$) transition.[17] For **YD2-o-C8**, its absorption spectrum features an intense Soret-band at 441 nm and less intense Q-bands at 577 and 641 nm. After photoexciting of this push-pull ZnP molecule at the Soret-band, it emits a single peak at 678 nm due to Q-band fluorescence. After substituting

the diarylamino functional group in **YD2-o-C8** with an ethynylene-bridged phenyl-Bodipy unit, **ZnP-dyad** exhibits panchromatic sensitization with an extended absorption onset at 765 nm from the Q-bands, a Soret-band at 455 nm, the $S_0 \rightarrow S_1$ ($^1\pi\pi^*$) transition from Bodipy moiety at 525 nm and a sharp Q-band at 659 nm. Basically, the absorption spectrum of **ZnP-dyad** is the sum of the two constituent chromophores and this outcome is similar to those of some other Bodipy-porphyrin light-harvesting arrays.[18] In addition, an extended shoulder peak among the Q-bands is located at 730 nm and this should originate from the elongated π-conjugation. Correspondingly, the peak located at the near-infrared region absorbs light beyond the typical metallated porphyrin chromophores. On the other hand, this dyad exhibits different photoluminescence spectra when excited at the Soret-band or the Bodipy-based absorption peak. When excited at the Soret band, this molecule emits strongly at 669 nm with a shoulder peak at 743 nm, both of which originate from the Q-bands. However, when it is excited at the Bodipy-based transition the dyad shows an additional emission peak with less intensity at 544 nm. The presence of the Q-band emission following excitation of the Bodipy reveals an energy transfer process from the peripheral Bodipy chromophore to the core ZnP chromophore whose energy transfer rate is comparable to the radiative lifetime of the Bodipy.

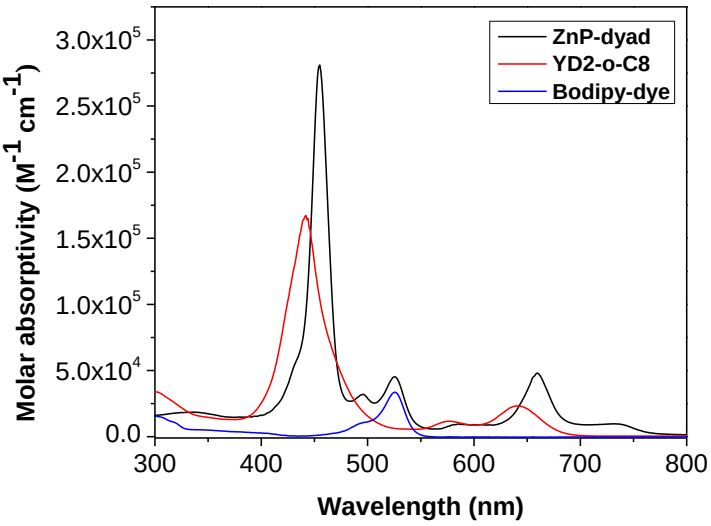

Figure 2. UV-vis absorption spectra of PSs **ZnP-dyad**, **YD2-o-C8** and **Bodipy-dye** in CH_2Cl_2 at ambient temperature.

Table 1. Absorption and emission data of **ZnP-dyad**, **YD2-o-C8** and **Bodipy-dye** in CH_2Cl_2.

Dye	λ_{abs} (ε [M^{-1} cm^{-1}]) [nm]	λ_{onset} [nm]	λ_{em} [nm]
ZnP-dyad	455 (281 000), 525 (45 300), 659 (48 100)	765	544, 669, 743
YD2-o-C8	441 (167 000), 577 (11 800), 641 (23 300)	685	678
Bodipy-dye	526 (33 700)	544	544

Electrochemical properties

Cyclic voltammetry (CV) measurements of these PSs focusing on positive applied potential (0–1.5 V vs SCE) were performed (Table 2). Cyclic voltammogram (Figure 3) of **Bodipy-dye** exhibits only one reversible oxidative wave ($E_{1/2}$ = 1.08 V) which corresponds to the formation of Bodipy radical cation.[19] For **YD2-o-C8**, it possesses two reversible oxidation peaks ($E_{1/2}$ = 0.54 V and 0.98 V), which both are originated from the oxidation of ZnP core and the

diarylamino moiety simultaneously.[13c] With regard to **ZnP-dyad**, its cyclic voltammogram is a sum of reversible oxidation of ZnP core ($E_{1/2}$ = 0.83 V) and Bodipy unit ($E_{1/2}$ = 1.09 V).[15]

As shown in Table 2, it is found that the E_{HOMO} of these PSs (–4.92 to –5.42 eV, relative to vacuum) are all more negative than the redox potential energy level (–4.65 eV, pH ~ 4) of ascorbic acid[20] (AA, as the sacrificial electron donor in H_2 production experiment) and the corresponding E_{LUMO} (–3.11 to –3.52 eV) are all higher than the conduction band energy level (~ –4.26 eV) of titanium dioxide nanoparticles.[21] Hence, effective dye regeneration[22] and electron injection[23] are both expected to proceed in the photocatalytic H_2 generation cycle.

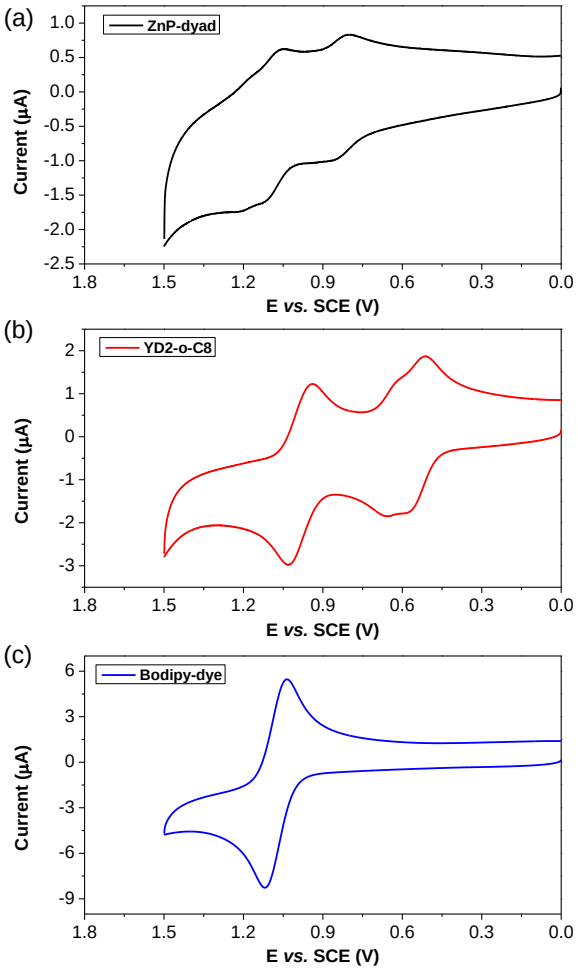

Figure 3. Cyclic voltammograms of (a) **ZnP-dyad**, (b) **YD2-o-C8** and (c) **Bodipy-dye** in dry CH_2Cl_2 using 0.1 M tetrabutylammonium hexafluorophosphate as supporting electrolyte with a scan rate of 0.1 V/s.

Table 2. Electrochemical data and energy levels of **ZnP-dyad**, **YD2-oC8** and **Bodipy-dye**.

Dye	E_{ox}[a] [V]	E_{HOMO}[b] [eV]	E_{0-0}[c] [eV]	E_{ox*}[d] [V]	E_{LUMO}[e] [eV]
ZnP-dyad	0.72	–5.14	1.62	–0.90	–3.52
YD2-o-C8	0.50	–4.92	1.81	–1.31	–3.11
Bodipy-dye	1.00	–5.42	2.28	–1.28	–3.14

[a] Half-wave oxidation potentials were measured by cyclic voltammetry in dry CH_2Cl_2 solution containing 0.1 M of $[NBu_4][PF_6]$ as the supporting electrolyte (vs. SCE reference electrode). Under these conditions, the reversible oxidation of ferrocene was $E_{1/2}$ = 0.38 V. [b] Calculated from – (E_{ox} + 4.42), as the E_{HOMO} of ferrocene is equal to –4.80 eV vs. to vacuum level. [c] E_{0-0} was determined from the onset of absorption spectrum. [d] $E_{ox*} = E_{ox} – E_{0-0}$. [e] $E_{LUMO} = E_{HOMO} + E_{0-0}$.

Computational studies

The ground state geometries of these PSs were optimized using DFT calculations (Figures 4, S13 and S14) and the dihedral angles between neighboring units are shown in Figure 5. From the results, the electron density in HOMO and LUMO of **Bodipy-dye** is localized at the Bodipy unit, whereas the anchor moiety is perpendicular to the plane of Bodipy unit and the π-conjugation is

disconnected at the twist point. For **YD2-o-C8**, the electronic density is distributed into the π-conjugation system of the ZnP core and diarylamino moiety in the HOMO, while the electron density in LUMO locates mainly in the ZnP core and phenylethynylene unit. This HOMO and LUMO configuration is anticipated to result in a prominent intramolecular charger-transfer (ICT) character for the excited dye, explaining the origin of push-pull character in this ZnP dye.[24] For **ZnP-dyad**, the electron density in the HOMO and LUMO is distributed primarily in the ZnP core and two phenylethynylene units. Notably, the plane of ZnP core is not coplanar with the two phenylethynylene units nor with the plane of Bodipy unit, hence direct communication of the π-electron density between ZnP core and Bodipy unit is expected to be insignificant.

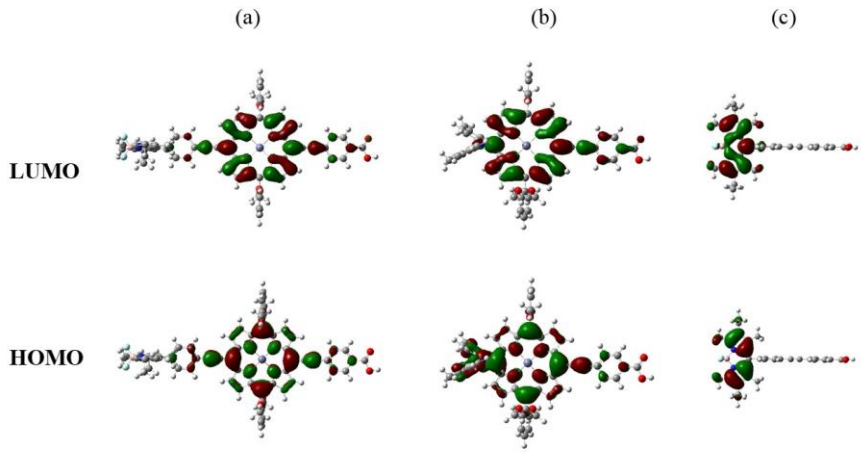

Figure 4. Selected molecular orbital diagrams for (a) **ZnP-dyad**, (b) **YD2-o-C8** and (c) **Bodipy-dye** obtained by DFT calculations with LC-wPBE. To simplify the calculations, alkyl chains on the photosensitizers are replaced with methyl groups.

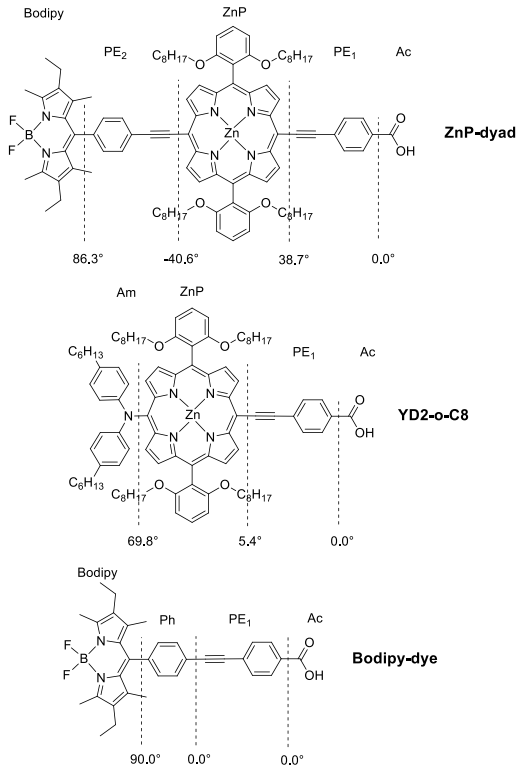

Figure 5. Dihedral angles between the neighboring units or between the phenylethynylene moiety and carboxylic acid in **ZnP-dyad**, **YD2-oC8** and **Bodipy-dye**, as determined by DFT geometry optimizations.

Transient absorption (TA)

Femtosecond TA control experiments of **Bodipy-dye** (Figure S17) and **YD2-o-C8**[25] confirmed prior observations of their excited state spectra and dynamics. **Bodipy-dye** exhibits transient signals that decay slowly with the $^1\pi\pi^*$'s 5-7 ns excited state lifetime, controlled by radiative and non-radiative internal conversion to the ground state.

The TA spectra of **ZnP-dyad** at each of the excitation wavelengths are shown in Figure 6. To fully map out the relaxation dynamics of **ZnP-dyad**, each of the three absorption bands (Figure 6a) were selectively probed via excitation at 650 nm, 520 nm and 470 nm (Figures 6b, 6c and 6d). Common to all the spectra, the ground state bleach (GSB) of both the Soret- and Q-bands are seen at 456 nm and 658 nm, respectively. A very broad excited state absorption (ESA)

from 468 nm into the near-IR is immediately present upon excitation of either of the porphyrin absorption bands. That broad ESA changes shape upon relaxation from the Soret state (the porphyrn S_2) into the Q-band state (the porphyrn S_1) and again at long times following intersystem crossing (ISC) to the triplet manifold. It should be noted that none of the transient spectra return to zero due to formation of a long-lived triplet state; however, all spectra do retain similar shape at long times, showing that regardless of excitation wavelength the molecule ends up in the same state: the T_1 state on the porphyrin. From the longtime decay kinetics, the lifetime of the lowest energy excited singlet was found to be 1300 ± 200 ps (see Figure S18), indicating a 0.77 ns^{-1} ISC rate.

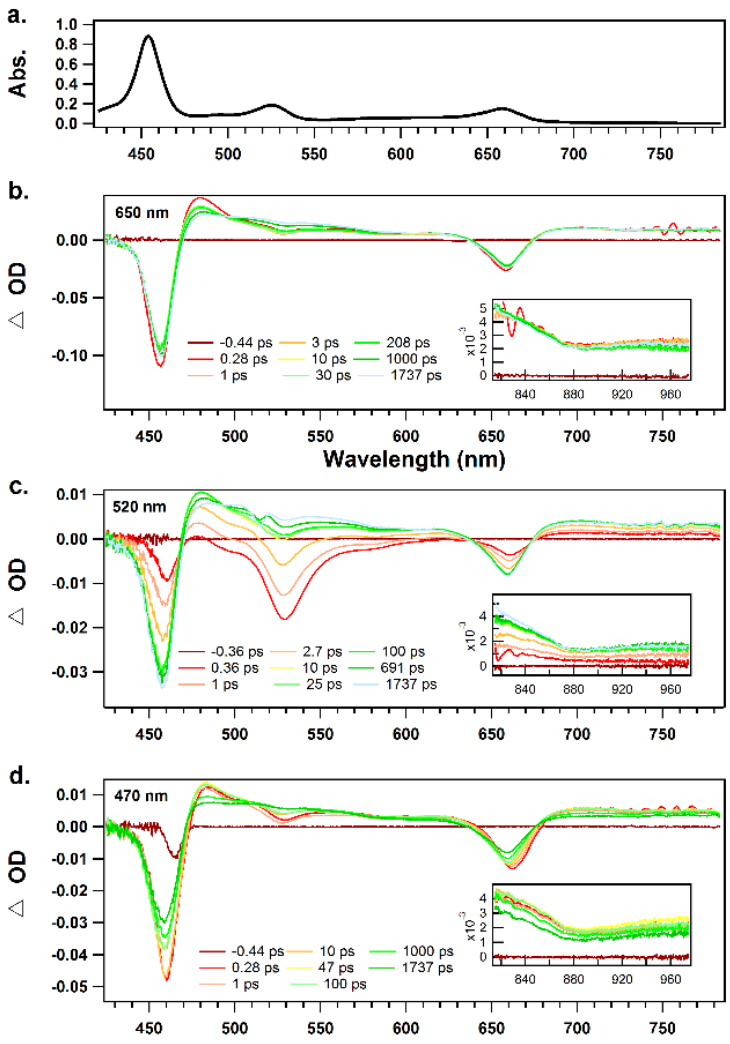

Figure 6. (a) The ground state absorption spectrum of **ZnP-dyad** in THF with the transient femtosecond transient absorption spectra with excitation at (b) 650 nm, (c) 520 nm and (d) 470 nm. NIR data is presented in the insets for each of the experiments.

Excitation with a 650-nm pump pulse was used to selectively excite the Q-band having a λ_{max} of 658 nm. This approach avoids populating the excited states of both the porphyrin S_2 transition (Soret-band) and the Bodipy antenna, allowing for observation of dynamics associated only with the lowest energy transition. As seen in Figures 6b and 7a, immediately following excitation, bleaches are apparent mirroring the ground state absorption for both the Soret and Q-band transitions. There is also an instantaneous appearance of the broad ESA that extends

throughout the probed spectral window, interrupted only by the porphyrin ground-state bleaches. Within the first 100–300 fs, the bleaches at 458 and 665 nm display a loss in amplitude while at 478 nm, the λ_{max} of the ESA, the signal rapidly decays with a 160-fs time constant. We attribute each of these 100–300 fs processes to ultrafast intramolecular reorganization of the excited state, combined with some degree of solvent reorganization. This reorganization is in agreement with the kinetics of the red-shift of negative signal at the Q-band wavelengths as ultrafast reorganization produces a minor Stokes shift in the Q-band stimulated emission. Following the ultrashort time dynamics, a third time constant of ~ 2 ps with extremely small amplitude attributed to vibrational relaxation within hot S_1 as seen with a narrowing and red-shift of the Q-band and lack of any dynamics associated with the Soret bleach. The small amplitude associated with this time constant is due to excitation near E_{00} of the Q-band resulting in only a small vibrationally excited population. Similar kinetics are found across the entire spectrum as the ESA extends to the NIR. A similar value of 2–6 ps has been reported by di Nunzio et. al. for the similar **YD2-o-C8** PS.[25] Lastly, we observe a loss of amplitude in the 478-nm shoulder of the ESA occurring with a 1300 ps time constant, indicating that the molecule undergoes ISC to the triplet manifold which then persists past the duration of the experiment.

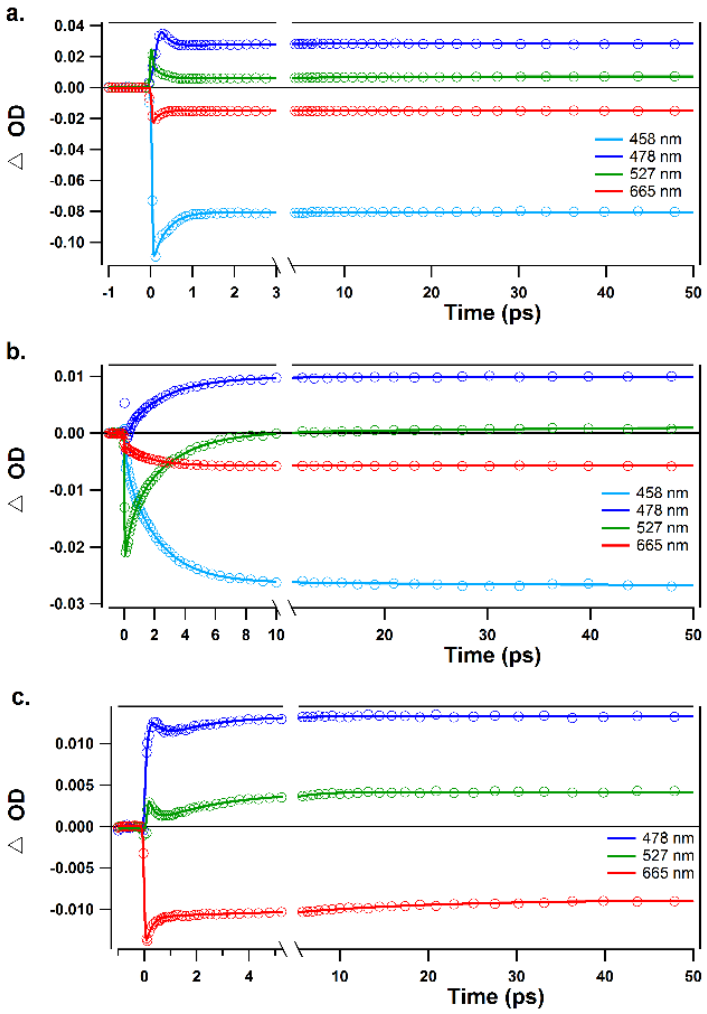

Figure 7. Kinetic fits of transient absorption signals of **ZnP-dyad** with excitation at (a) 650 nm, (b) 520 nm and (c) 470 nm.

A 520 nm pump pulse was used to selectively excite the Bodipy moiety separate from the porphyrin bands (Figure 6c). Following laser excitation, an immediate bleach was formed centered at 527 nm, similar to that of excitation of **Bodipy-dye** as seen in Figure S17. At early times, a slight ultrafast (300–500 fs) attenuation is seen at wavelength of 478 nm and 527 nm characteristic of vibrational cooling of the Bodipy moiety. Following this process, the bleach at 527 nm losses all its amplitude with a 2.3 ps time constant while both the Soret- and Q-band bleaches appear with similar time constants. ESA to the red of the Q-band bleach, and in the

near-IR (inset of Figure 6c), which has been attributed to the ESA from the Q-band population, increases in amplitude as the Q-band bleach forms. As seen in Figure 7b, the signal is dominated by the large amplitude associated with this time constant which we attribute to efficient energy transfer from the Bodipy to the porphyrin moiety in 2.3 ps. Interestingly, vibrational relaxation (VR) of the excited porphyrin following the energy transfer is not observed since VR occurs at the same rate as or slightly faster than the energy transfer.

To see if energy transfer is possible from the Soret-band into the Bodipy moiety, excitation of the S_2 transition was accomplished with a pump pulse of 470 nm overlapping with the red-edge of the Soret-band. Immediately following excitation, bleaches at the Soret- and Q-bands are formed with a minor bleach of the Bodipy formed at 527 nm. By quantifying each of these signals over the first ~10 ps (see details in Supporting Information), we can determine that 94% of the pump pulse absorption occurs to the Soret-band and just 6% of the pump-induced absorptions excite the Bodipy directly.

The earliest time dynamics show a slight decrease in amplitude in both the Soret- and Q-band bleaches with a simultaneous increase of the bleach at 527 nm, all occurring with an average time constant of 280 fs. We assign this to energy transfer from the higher energy Soret-band to the Bodipy moiety occurring at the same time as internal conversion from the Soret-band to the Q-band. Quantification of these dynamics can be found in the Supporting Information and shows that within 300 fs 87% of the excited the Soret population undergoes IC to the Q-band and 13% undergoes energy transfer into the Bodipy moiety. In the subsequent ~2.5 ps the blue side of the spectrum shows an increase in bleach of the Soret-band while a loss is seen at the shoulder of the ESA centered at 478 nm. Within this same time constant, a growth of a new broadly absorbing ESA is observed covering most of the spectrum while a loss in bleach amplitude of the

Q-band occurs. The loss of signal at 478 nm has been attributed to loss of the Soret to S_n transition whilst the loss in bleach at 665 nm is the result of the overlap with the Q-band bleach and the newly formed absorption of the S_1-S_n state. We attribute the shorter time constant (~100 fs) to simultaneous internal conversion from the Soret to the Q-band and energy transfer from the Soret to Bodipy and we attribute the longer time constant (~ 2.5 ps) to energy transfer from the excited Bodipy to the Q-band.

Lastly, we should note that there is no evidence at any excitation wavelength for triplet energy transfer (TEnT) from the ZnP to the Bodipy, which would be visible in a long-term bleach of the Bodipy absorption band. This indicates that the orbitals localized on either portion of the dyad are well insulated from each other, providing no orbital overlap necessary for TEnT. However, we cannot rule out the occurrence of TEnT on time-scales much longer than the 2-ns TA experiment.

Photocatalytic hydrogen generation

In view of the panchromatic light-absorbing properties of **ZnP-dyad** and **YD2-o-C8**, we exploited these PSs to study light-driven H_2 generation from water based on PS-TiO_2-Pt nanocomposite materials. In particular, both green and white lights supplied by light-emitting diode (LED) light sources were utilized to examine the effectiveness of ZnP chromophore and Bodipy-based antenna design in promoting the photoelectrochemical process. Comparisons of the UV-vis spectra in THF solutions of **ZnP-dyad**, **YD2-o-C8** and **Bodipy-dye** before and after sonication in the presence of platinized TiO_2, are used to determine the extent of binding of the PS onto the TiO_2 particles. (The corresponding spectra are displayed in Figures S20–S24.) The relatively low dye-loading values (ca. 40–70%) as compared to the previous reports[8a, 9] are

probably ascribed to the larger molecular size of PSs in this study. In short, the H_2 generation experiments were conducted on aqueous solutions at pH 4.0 with ascorbic acid (AA, 0.5 M) serving as the hole scavenger. Similar to previous reports, gas chromatography (GC) analysis based on a methane internal standard calibration method was used to measure the H_2 amount (Figure S25) at the end of the irradiation. Detailed procedures can be found in the Experimental section.

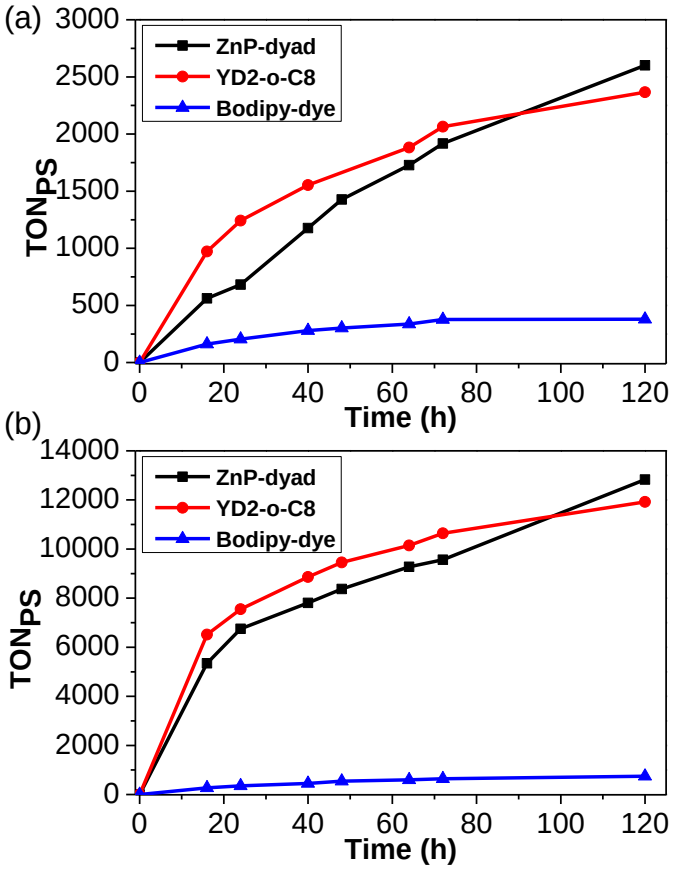

Figure 8. Photocatalytic H_2 evolution with respect to different PSs under irradiation of (a) green LED (520 nm) at 50 mW and (b) white LED (420–750 nm) at 80 mW. Each sample consisted of 5 mL of 0.5 M AA in water at pH 4.0, with 20 mg of PS-TiO_2-Pt composite material was introduced.

Table 3. Light-driven H_2 generation data with and without PSs.

Dye	DL%[a]	H_2 [mL]	TON[b]	TOF[c] [hr^{-1}]	TOF_i[d] [hr^{-1}]	$Activity_i$[e] [μmol g^{-1} hr^{-1}]	AQY_i%[f]
				Green LED			
ZnP-dyad	41.3	3.22	2600	21.7	35.1	18100	0.464
YD2-o-C8	62.8	4.45	2370	19.8	60.8	47700	1.22
Bodipy-dye	71.1	0.81	379	3.2	10.1	9020	0.231
none	0	0.45[g]	–	–	–	9200	0.235
				White LED			
ZnP-dyad	41.5	15.95	12800	107	334	173000	2.59
YD2-o-C8	53.5	19.11	11900	99.2	407	272000	4.07
Bodipy-dye	71.1	1.59	744	6.2	17.1	15200	0.228
none	0	2.33	–	–	–	23100	0.346

[a] Dye-loading percentage. [b] Turnover number (TON) of H_2 is calculated as number of mole of H_2 produced divided by the number of mole of PS attached to platinized TiO_2. [c] Turnover frequency (TOF) is calculated as TON divided by the number of hours (i.e. 120 hours). [d] Initial turnover frequency (TOF_i) in the first 16 hours. [e] Initial photocatalytic activity ($Activity_i$) of the system is defined as number of micromole of H_2 evolved per gram of platinum loaded per hour. [f] Initial apparent quantum yield percentage (AQY_i%) of the system. [g] 48 hours were taken instead of 120 hours.

Plots of H_2 TON vs irradiation time (120 h) for **ZnP-dyad**, **YD2-o-C8** and **Bodipy-dye** are depicted in Figure 8, and the corresponding data (TON, TOF, TOF_i, $Activity_i$ and AQY_i%) are exhibited in Table 3. Under green light irradiation, both ZnP-containing PSs (**ZnP-dyad** and **YD2-oC8**) promote photocatalytic H_2 generation (> 3 mL), while the **Bodipy-dye** does not function and its PS-TiO_2-Pt composite material only renders the same result as the bare TiO_2-Pt composite control affords, according to their initial activity ($Activity_i$) and apparent quantum yield (AQY_i%). Overall, **ZnP-dyad** and **YD2-o-C8** attain TONs of 2600 and 2370, respectively, but **YD2-o-C8** yields an almost double initial TOF of 60.8 hr^{-1}. Under white light irradiation, the

three PSs exhibit a similar pattern of activity, whereas both ZnP-containing PSs potently facilitate the light-driven H_2 generation (> 16 mL) and **Bodipy-dye** remains inactive (~ 2 mL) in the photocatalytic reaction. The systems with **ZnP-dyad** and **YD2-o-C8** afford high photocatalytic activity over 120 h with TONs of 12800 and 11900, respectively, while **YD2-o-C8** achieves a remarkable TOF_i larger than 400 hr^{-1} and **ZnP-dyad** also reaches a TOF_i of 334 hr^{-1}.

Under both green- and white-light irradiation, the resultant H_2 generation of **Bodipy-dye**-based system is essentially the same as the control. This indicates the dye-sensitization approach is not effective though Bodipy chromophore is highly light-absorbing in 500–550 nm. For instance, another structurally similar Bodipy-based sensitizer demonstrated a poor efficiency of electron injection in another study[26], while Ziessel et al. proposed that the di-substitution of long alkoxyl groups to the 4-position of Bodipy chromophore via carbon-carbon triple bonds could ameliorated the charge recombination with TiO_2.[27] According to the computational studies (Figure 4c), the HOMO and LUMO both stay at the center of **Bodipy-dye** chromophore and, presumably, the phenylethynylene moiety and the adjoining phenyl ring act like an insulating layer and block the photoinduced electron injection into TiO_2, due to the disconnection of π-conjugation. Therefore, even when intense green light is used to photoexcite the PS, the light-harvesting effect by the organic PS still remains minimal.

Conversely, both ZnP-containing PSs possess a certain degree of LUMO at the anchor-adjoining phenylethynylene moiety (see Figures 4a and 4b), ensuring an effective photoinduced electron injection into the conduction band of TiO_2 from both **ZnP-dyad** and **YD2-o-C8**. As a result, the dye-sensitization approach is effective for these two PSs and the production of H_2 is realized in both of cases. The two PSs generate approximately 5 times more H_2 under white light

irradiation than under green light, when comparing final TON values. Additionally, the initial TOF is 4-6 times larger under white-light illumination, even after the 60% larger intensity of the white-light LED compared to the green LED is taken into account. Consequently, the significant differences in turnover reveal the benefit of developing panchromatic dyes for photocatalytic reactions, especially in the considerations of solar-driven water splitting reaction and related photocatalysis.[28],[29]

From the TA result, a 2.3 ps time constant is assigned for the singlet energy transfer from the Bodipy unit to the ZnP moiety, comparable to those (i.e. 0.51–0.73 ps) of the reported Bodipy-conjugated PtN_2S_2 PSs. In the Bodipy-PtN_2S_2 systems, the Bodipy-antenna is an effective energy transfer chromophore towards the PtN_2S_2 charge-transfer moiety, hence raising up the H_2 production efficiency.[10b, 30] Accordingly, our dyad design should give a positive contribution towards the H_2 generation compared to ZnP alone. In addition, Hupp et al. in 2009 reported that a similar Bodipy-conjugated ZnP dyad (structure shown in Figure S29) exhibited higher incident photon-to-current efficiencies in the range of 500–550 nm as compared to another ZnP-based PS without the Bodipy unit (structure shown in Figure S29), for the corresponding DSSCs.[15] In brief, the Bodipy unit was shown to facilitate light-harvesting using the dyad approach, in agreement with the efficacy observed for our **ZnP-dyad** towards hydrogen production, which depends on the same electron injection processes as the prior DSSC study by Hupp.

On the basis of structural consideration, push-pull type **YD2-o-C8** PS is different from **ZnP-dyad** with the presence of diarylamino moiety, which has been proven to provide a strong electron-donating strength towards the ZnP unit in some previous studies by Yeh, Diau and co-workers.[13a, 13b] Thus, the electron injection step for **YD2-o-C8** is anticipated faster than that of

ZnP-dyad because of the strong charge pushing effect.[31] Additionally, the hole in the HOMO on **YD2-o-C8** will be localized further away from the surface of TiO_2, potentially slowing down back electron transfer from the semiconductor and enhancing overall efficiency.

However, when the white light irradiation is exploited, the stronger light absorbing capability throughout the visible light region of **ZnP-dyad** relative to **YD2-o-C8** (see Figure 2) compensates the poorer charge separation effectiveness, and this leads to almost the same TOF_i for these two ZnP-containing PSs.

Conclusion

In summary, we report the use of ZnP-sensitized platinized TiO_2 for light-driven hydrogen generation from aqueous media. The absorption spectrum of the Bodipy-conjugated **ZnP-dyad** successfully intensifies and extends the absorption throughout the visible region, especially filling up the weak absorption in the range of 500–550 nm of **YD2-o-C8** and other porphyrins. Ultrafast transient absorption spectroscopy is used to determine that the time constant for the singlet energy transfer from the Bodipy unit to ZnP chromophore is 2.3 ps, supporting the possibility to utilize the energy transferred from Bodipy chromophore for effective charge separation at the interface between PS and TiO_2. However, the photocatalytic system with **YD2-o-C8** still performs better than that of **ZnP-dyad** and gives an almost double value of TOF_i under green light excitation, this comparison indicates that the electronic push-pull configuration plays a pivotal role for ZnP PS at the charge separation interface. On the other hand, both ZnP-containing PSs render much higher initial TOFs and total TONs when green light is changed to white light irradiation. This result clearly demonstrates the importance and advantage of panchromatic sensitization. In this regard, **YD2-o-C8** achieved a very active H_2 generation

system with a TOF_i of 407 h^{-1} and a total TON of around 12000 over 120 h. Notably, this pilot study, which focuses on panchromatic ZnP PSs, paves the way in improving the photocatalytic system, especially in the context of solar-driven H_2 production and other related photocatalytic reactions.

Experimental Section

General

All chemical reactions were performed under an inert nitrogen atmosphere with the use of a Schlenk line. Glassware was dried in oven prior to use. Commercially available reagents were used without purification. All the reagents for chemical synthesis were purchased from Tokyo Chemical Industry Co., Ltd (TCI), Sigma-Aldrich, Acros Organics or Dieckmann. Solvents were dried by distillation over suitable drying agents. PS **YD2-o-C8** was purchased from Yingkou OPV Tech New Energy Co., Ltd. All the reactions were monitored by thin-layer chromatography (TLC) with Merck pre-coated aluminium plates. Products were purified by column chromatography on silica gel (230−400 mesh) purchased from Merck.

Characterization

Proton and carbon NMR spectra were measured in $CDCl_3$ or THF-d_8 on a Bruker Ultra-shield 400 MHz FT-NMR spectrometer and tetramethylsilane (TMS) was exploited as an internal standard for calibrating the chemical shift. Matrix-assisted laser desorption ionization time-of-flight (MALDI-TOF) mass spectrometry was performed on an Autoflex Bruker MALDI-TOF system. UV/Vis absorption spectroscopy was performed on a Hewlett Packard 8453 spectrometer in dichloromethane solution at 293 K. The solution emission spectra and lifetimes

of the PSs were measured on a Perkin Elmer LS50B spectrophotometer at 293 K. Electrochemical measurements were conducted on a CHI 630C Electrochemical Analyzer/Workstation at a scan rate of 100 mV s^{-1}.

Preparation of platinized TiO_2

For a 0.5 wt-% platinized TiO_2 sample, addition of 40 mL methanol to 1.6 g of titanium(IV) oxide nanopowder (anatase, < 25 nm particle size, 99.7% trace metals basis, Sigma-Aldrich) and 0.1 mL of H_2PtCl_6 aqueous solution (8 wt. %) created slurry which was then subjected to radiation from a 300 W coated Hg lamp (HF300PD, EYE Lighting) under vigorously stirring for 24 hours. The resulting crude product had a grayish colour. Platinized TiO_2 was then retrieved by centrifugation at 3500 rpm for 5 minutes and washed three times with methanol. The obtained material was dried under vacuum at ~ 60 °C in darkness for eight hours.

Adsorption of photosensitizer onto platinized TiO_2

20 mg of the prepared platinized TiO_2 was added to 2.5 mL of 50 μM PS THF solution, the mixture was then sonicated for 30 minutes. The solution lost colour gradually while the solid became pink or dark-green. The dye-loaded solid was then retrieved by centrifugation at 3500 rpm for 5 minutes. The supernatant layer solvent was removed carefully using a dropper and the pellet at the bottom was dried under vacuum for two to three hours in darkness. At the end, the whole dried pellet was directly utilized in the photocatalytic reaction mixture for one photolysis experiment without further characterization.

The dye loading percentage, DL%, for each PS was estimated by comparing the absorbance value of absorption peak with the highest ε before and after the dye adsorption (Table

3). The corresponding UV/vis spectra for **ZnP-dyad**, **YD2-o-C8** and **Bodipy-dye** are shown in Figures S20–S24, respectively.

Light-driven hydrogen production studies

The photocatalytic reactions were carried out in 5 mL aqueous ascorbic acid (AA, 0.5 M) solution at pH 4.0 with AA serving as the SED (AA is selected in our system, because its relationship between pH value and H_2-evolving activity has been studied in details very recently and the redox chemistry is also well-known[32]). A 25 mL pear-shaped flask was placed above stirrers at 19 °C and the flask was sealed with rubber septa. The photocatalytic reaction mixture with a stir bar was then purged with a mixture of gas containing argon/methane (80:20 mol%) for 15 minutes. The methane present in the gas mixture was served as an internal standard for GC analysis at the end of each experiment. The reaction mixture was steadily stirred and continuously radiated from the bottom with green (ca. 520 nm) and white light-emitting diodes (420–750 nm) inside a just-fit container which blocks the stray light from the environment. The light power was measured with a thermal sensor (Model: BIM-7203-0100F) and power meter (Model: BIM-7001; Hangzhou Brolight Technology Co., Ltd.), and estimated to be ~ 50 mW (green light) and ~ 80 mW (white light) for each reaction mixture. At the end of the experiment, the headspaces of the flasks were characterized by GC to examine the amount of hydrogen produced. The amounts of hydrogen evolved were determined by using GC (Shimadzu GC-8A with a molecular sieve 5 Å column and TCD detector) at the end of the radiation period and were quantified using a calibration plot of integrated amount of hydrogen relative to the methane (Figure S25). In the course of radiation, GC samples were taken at different time points. The LED radiation is assumed to be monochromatic at emission intensity maximum (520 nm for

green light; 556 nm for white light) and the corresponding apparent quantum yield values for each photosensitizer could be estimated according to the equation shown below.

$$\text{AQY}\ (\%) = \frac{\text{rate of } H_2 \text{ production} \times 2}{\text{rate of incident photons}} \times 100\%$$

Synthetic procedures of intermediates and PSs

Compound 1

3-Ethyl-2,4-dimethyl-1*H*-pyrrole (950 mg, 7.72 mmol), 4-iodobenzoyl chloride (1.03 g, 3.87 mmol) and dry CH_2Cl_2 (50 mL) were stirred in dark overnight at 25 °C. NEt_3 (2.5 mL) was then added. After 10 min, boron trifluoride etherate (2.5 mL, 20.13 mmol) was introduced and the reaction mixture was stirred for an hour. The crude mixture was purified by column chromatography on silica gel, and the product band was eluted out using CH_2Cl_2/hexane (1:1, v/v) as an eluent. Recrystallization of the product using CH_2Cl_2/diethyl ether was performed to yield compound **1** as a red solid (413 mg, 0.79 mmol, 20%). ^{1}H NMR ($CDCl_3$, 400 MHz): δ = 7.85−7.82 (m, 2H, Ar), 7.04 (d, 2H, J = 8.4 Hz, Ar), 2.53 (s, 6H, alkyl), 2.30 (q, 4H, J = 7.6 Hz, alkyl), 1.32 (s, 6H, alkyl), 0.98 (t, 6H, J = 7.6 Hz, alkyl); ^{13}C NMR (100 MHz, $CDCl_3$): δ = 154.15, 138.52, 138.25, 138.17, 135.38, 133.03, 130.49, 130.29, 94.51 (Ar), 17.08, 14.64, 12.56, 11.99 ppm (alkyl). HRMS (MALDI-TOF, *m*/*z*): [M^+] 506.1205; calcd for ($C_{23}H_{26}BF_2IN_2$) 506.1202.

Compound 2

A mixture of **1** (60 mg, 0.119 mmol), trimethylsilylacetylene (0.05 mL), $Pd(PPh_3)_2Cl_2$ (7 mg, 0.009 mmol) and CuI (2 mg, 0.009 mmol) in a mixture of THF/NEt_3 (10/1, 22 mL) was heated to reflux under nitrogen atmosphere overnight. The solvent was removed under reduced pressure. The residue was purified by column chromatography on silica gel using a 1:2 mixture of CH_2Cl_2

and hexane as eluent to afford compound **2** (52 mg, 0.088 mmol, 74%) as a red solid. ^{1}H NMR ($CDCl_3$, 400 MHz): δ = 7.60 (d, 2H, *J* = 8.4 Hz, Ar), 7.24 (d, 2H, *J* = 8.4 Hz, Ar), 2.53 (s, 6H, alkyl), 2.30 (q, 4H, *J* = 7.6 Hz, alkyl), 1.29 (s, 6H, alkyl), 0.98 (t, 6H, *J* = 7.6 Hz, alkyl), 0.29 (s, 9H, $Si(CH_3)_3$); ^{13}C NMR (100 MHz, $CDCl_3$): δ = 154.01, 139.20, 138.23, 136.08, 132.92, 132.65, 130.49, 128.38 (Ar), 104.36, 95.61 (C≡C), 17.07, 14.64, 12.54, 11.91 (alkyl), −0.07 ppm ($Si(CH_3)_3$). HRMS (MALDI-TOF, *m*/*z*): [M^+] 592.2420; calcd for ($C_{30}H_{41}BCl_2F_2N_2OSi$) 592.2426.

Compound 3

To a flask containing the ethynyl precursor (52 mg, 0.109 mmol) and K_2CO_3 (151 mg, 1.09 mmol) was added 22 mL of CH_2Cl_2/CH_3OH (10:1, v/v). The solution was allowed to stir at room temperature for 3 h. The solvents were then removed by evaporation under reduced pressure, and the residue was extracted with CH_2Cl_2 and washed with water (3 × 20 mL). The organic layer was evaporated under reduced pressure, and was purified by column chromatography on silica gel using a mixture of hexane/CH_2Cl_2 (1:1, v/v) as eluent to obtain a red solid (24 mg, 0.059 mmol, 54%). ^{1}H NMR ($CDCl_3$, 400 MHz): δ = 7.63−7.61 (m, 2H, Ar), 7.28−7.26 (m, 2H, Ar), 3.19 (s, 1H, C≡C−H), 2.53 (s, 6H, alkyl), 2.30 (q, 4H, *J* = 7.6 Hz, alkyl), 1.30 (s, 6H, alkyl), 0.98 (t, 6H, *J* = 7.6 Hz, alkyl); ^{13}C NMR (100 MHz, $CDCl_3$): δ = 154.09, 139.01, 138.20, 136.45, 132.97, 132.79, 130.48, 128.51, 122.67 (Ar), 83.03, 78.43 (C≡C), 17.08, 14.64, 12.55, 11.89 ppm (alkyl). HRMS (MALDI-TOF, *m*/*z*): [M^+] 404.2239; calcd for ($C_{25}H_{27}BF_2N_2$) 404.2235.

PS ZnP-dyad

Protected di-ethynyl precursor **ZnP** (54 mg, 0.039) was dissolved in 20 mL THF, the solution was then cooled in an ice bath followed by the addition of tetra(*n*-butyl)ammonium fluoride (1M in THF, 0.39 mL, 0.386 mmol). After being stirred for one hour, the solution was evaporated

under reduced pressure. The resulting residues were extracted with CH_2Cl_2 and washed with water (3 × 20 mL). The solvent was evaporated under reduced pressure followed by re-dissolving it into 25 mL mixture of THF/NEt_3 (2:3, v/v) and subsequently cooled in an ice-bath. To this reaction mixture, compound **1** (20 mg, 0.039 mmol), 4-iodobenzoic acid (10 mg, 0.039 mmol), $Pd_2(dba)_3$ (2 mg, 0.002 mmol), PPh_3 (1 mg, 0.04 mmol) and CuI (1 mg, 0.002 mmol) were added. The reaction mixture was stirred at 0 °C for 30 min and then refluxed overnight (the temperature was increased slowly). After the solvent was removed under reduced pressure, the residue was purified by column chromatography on silica gel using pure CH_2Cl_2, and the product band was eluted out using CH_2Cl_2/CH_3OH (19:1, v/v) solution mixture to afford a dark solid. This solid was further purified by precipitation using CH_2Cl_2/hexane and the precipitate was dried under vacuum to yield the PS **ZnP-dyad** (32 mg, 0.020 mmol, 51%) as a dark solid. ^{1}H NMR ($CDCl_3$, 400 MHz): δ = 9.72 (d, 2H, *J* = 4.8 Hz, Ar), 9.67 (d, 2H, *J* = 4.8 Hz, Ar), 8.91−8.90 (m, 4H, Ar), 8.21 (d, 2H, *J* = 8 Hz, Ar), 8.14 (d, 2H, *J* = 8.4 Hz, Ar), 8.06 (d, 2H, *J* = 8.4 Hz, Ar), 7.75−7.71 (m, 2H, Ar), 7.49 (d, 2H, *J* = 8 Hz, Ar), 7.03 (d, 4H, *J* = 8.4 Hz, Ar), 3.88 (t, 8H, *J* = 6.4 Hz, alkyl), 2.58 (s, 6H, alkyl), 2.37−2.34 (m, 4H, alkyl), 1.26 (s, 6H, alkyl), 1.05−0.97 (m, 14H, alkyl), 0.85−0.80 (m, 8H, alkyl), 0.66−0.49 (m, 8H, alkyl), 0.45−0.38 (m, 36H, alkyl); ^{13}C NMR (100 MHz, $CDCl_3$): δ = 159.86 (COOH), 154.01, 151.68, 151.53, 150.75, 139.58, 138.42, 135.56, 132.98, 132.19, 132.05, 130.71, 130.52, 129.96, 128.76, 125.17, 120.66, 115.65, 105.18 (Ar), 99.99, 99.31, 95.11, 94.60 (C≡C), 68.61, 31.39, 29.71, 29.66, 29.61, 29.46, 29.37, 29.33, 29.10, 28.73, 28.65, 28.58, 27.21, 25.26, 22.29, 17.13, 14.67, 13.85, 12.59, 12.06 ppm (alkyl). HRMS (MALDI-TOF, *m*/*z*): [$(M+H)^+$] 1584.8108; calcd for ($C_{98}H_{114}BF_2N_6O_6Zn$) 1584.8186.

PS Bodipy-dye

A mixture of **3** (24 mg, 0.059 mmol), 4-iodobenzoic acid (13 mg, 0.050 mmol), $Pd_2(dba)_3$ (3 mg, 0.003 mmol), PPh_3 (1.5 mg, 0.06 mmol) and CuI (1 mg, 0.003 mmol) in a mixture of THF/NEt_3 (20/1, 21 mL) was heated to reflux under nitrogen atmosphere overnight. The solvent was removed under reduced pressure. After the removal of solvent, the impurities were removed by column chromatography on silica gel using pure CH_2Cl_2, and the product band was eluted out using CH_2Cl_2/CH_3OH (10:1, v/v) solution mixture to afford photosensitizer **Bodipy-dye** (24 mg, 0.046 mmol, 78%) as a red solid. ^{1}H NMR (THF-d_8, 400 MHz): δ = 8.04 (d, 2H, J = 6.8 Hz, Ar), 7.73 (d, 2H, J = 8.4 Hz, Ar), 7.64 (d, 2H, J = 7.6 Hz, Ar), 7.41 (d, 2H, J = 8 Hz, Ar), 2.49 (s, 6H, alkyl), 2.34 (q, 4H, J = 7.6 Hz, alkyl), 1.38 (s, 6H, alkyl), 0.99 (t, 6H, J = 7.6 Hz, alkyl); ^{13}C NMR (100 MHz, THF-d_8): δ = 153.74, 139.53, 137.56, 136.47, 132.56, 132.21, 131.24, 130.39, 129.66, 128.89, 127.07, 123.51 (Ar), 91.04, 89.57 (C≡C), 16.69, 14.00, 11.59, 11.15 ppm (alkyl). HRMS (MALDI-TOF, m/z): [M^+] 524.2489; calcd for ($C_{32}H_{31}BF_2N_2O_2$) 524.2447.

Transient absorption

A regeneratively amplified titanium:sapphire laser (Spectra-Physics Spitfire) was used to produce femtosecond laser pulses at a 1 kHz repetition rate. The pump pulse was produced from a home-built noncollinear optical parametric amplifier (NOPA) centered at three different wavelengths of 470 nm, 520 nm and 650 nm with a pulse energy of 100 nJ per pulse and a bandwidth of 14 nm, 11 nm and 40 nm, respectively.[33] A mechanical chopper was used to block every other pump pulse. The probe beam was created by focusing of the fundamental 800 nm beam through either a sapphire crystal to produce a white light continuum spanning 425 nm to 950 nm or through calcium fluoride (CaF_2) giving a continuum from 350 nm to 650 nm. The probe was dispersed by a grating spectrograph (Acton, 300mm fl, 150gr/mm) before reaching the CCD camera (Princeton Instruments, Pixis 100BR). The white light spectrum was filtered using

a dye solution (NIR800A, QCR Solutions Corp) to block residual 800 nm light from entering the spectrograph during sample collection and a 780-nm long pass when collecting signal in the near-infrared (NIR). Solution samples were prepared in a 2-mm fused-silica cuvette and diluted to an absorbance of ~0.1-0.7 and the cuvettes were translated vertically at ~2 mm/s to refresh the illuminated sample. TA signal was collected using both parallel and perpendicular pump to probe polarizations, with the isotropic (magic angle) signal calculated via:

$$\Delta A_{Iso} = \frac{(\Delta A_{\parallel} + 2\Delta A_{\perp})}{3}$$

Kinetic data was fit to a series of exponentials with varying amplitudes, convoluted with a Gaussian instrument response function that was established by the pump-probe cross-correlation. Cross-correlations (XC) were determined from Optical Kerr Effect (OKE) signals obtained when pump and probe were overlapped in a 1-mm glass slide. OKE signals were averaged over all wavelengths of interest giving values of 100 fs, 60 fs and 50 fs for excitation wavelengths of 470 nm, 520 nm and 650 nm, respectively.

Computational studies

Density functional theory (DFT) calculations and time-dependent density functional theory (TD-DFT)[34] calculations provide useful information for the nature of electronic ground states and excited states, respectively. Both DFT and TD-DFT calculations were performed by using the Gaussian 09 package.[35] The B3LYP[36] hybrid functional with 20% Hatree-Fock exchange and LC-wPBE functional were used. The 6-31G(d,p) basis set was used for C, H, B, F, N, O, S, and Zn. The optimized geometries for **ZnP-dyad**, **YD2-o-C8** and **Bodipy-dye** were confirmed with all real frequencies.

Acknowledgements

C.-L. Ho thanks the Hong Kong Research Grants Council (PolyU 123021/17P), National Natural Science Foundation of China (21504074), the Science, Technology and Innovation Committee of Shenzhen Municipality (JCYJ20160531193836532) and the Hong Kong Polytechnic University (1-BE0Q) for financial their financial support. M.F.M., D.W.M. and R.E. were supported by a grant from the U.S. National Science Foundation's Chemical Catalysis division under Collaborative Research Grant CHE- 1566080. We are thankful to Jacob Shelton and Kathryn Knowles at the University of Rochester for their assistance with the diffuse reflectance measurements.

Conflict of interest

The authors declare no conflict interest.

Keywords: hydrogen production · photosensitizer · Zn(II) porphyrin · transient absorption · photocatalysis

References

[1] S. Chu, A. Majumdar, *Nature* **2012**, *488*, 294–303.

[2] a) J. Lelieveld, J. S. Evans, M. Fnais, D. Giannadaki, A. Pozzer, *Nature* **2015**, *525*, 367–371; b) C. McGlade, P. Ekins, *Nature* **2015**, *517*, 187–190.

[3] a) T. Hisatomi, J. Kubota, K. Domen, *Chem. Soc. Rev.* **2014**, *43*, 7520–7535; b) N. S. Lewis, D. G. Nocera, *Proc. Natl. Acad. Sci. U. S. A.* **2006**, *103*, 15729–15735; c) H. Ahmad, S. K. Kamarudin, L. J. Minggu, M. Kassim, *Renewable Sustainable Energy Rev.*

2015, *43*, 599–610; d) Z. Li, W. Luo, M. Zhang, J. Feng, Z. Zou, *Energy Environ. Sci.* **2013**, *6*, 347–370.

[4] P. V. Kamat, J. Bisquert, *J. Phys. Chem. C* **2013**, *117*, 14873–14875.

[5] G. Centi, S. Perathoner, *Green carbon dioxide: advances in CO2 utilization*, John Wiley & Sons, **2014**.

[6] a) A. J. Bard, M. A. Fox, *Acc. Chem. Res.* **1995**, *28*, 141–145; b) L.-Z. Wu, B. Chen, Z.-J. Li, C.-H. Tung, *Acc. Chem. Res.* **2014**, *47*, 2177–2185; c) J. J. Concepcion, J. W. Jurss, M. K. Brennaman, P. G. Hoertz, A. O. T. Patrocinio, N. Y. Murakami Iha, J. L. Templeton, T. J. Meyer, *Acc. Chem. Res.* **2009**, *42*, 1954–1965.

[7] W. T. Eckenhoff, R. Eisenberg, *Dalton Trans.* **2012**, *41*, 13004–13021.

[8] a) P.-Y. Ho, Y. Wang, S.-C. Yiu, W.-H. Yu, C.-L. Ho, S. Huang, *Org. Lett.* **2017**, *19*, 1048–1051; b) W. J. Youngblood, S. H. Lee, Y. Kobayashi, E. A. Hernandez-Pagan, P. G. Hoertz, T. A. Moore, A. L. Moore, D. Gust, T. E. Mallouk, *J. Am. Chem. Soc.* **2009**, *131*, 926–927; c) L. Li, L. Duan, Y. Xu, M. Gorlov, A. Hagfeldt, L. Sun, *Chem. Commun.* **2010**, *46*, 7307–7309; d) E. D. Cline, S. E. Adamson, S. Bernhard, *Inorg. Chem.* **2008**, *47*, 10378–10388; e) P. Du, K. Knowles, R. Eisenberg, *J. Am. Chem. Soc.* **2008**, *130*, 12576–12577; f) P. Jarosz, P. Du, J. Schneider, S.-H. Lee, D. McCamant, R. Eisenberg, *Inorg. Chem.* **2009**, *48*, 9653–9663; g) P. N. Curtin, L. L. Tinker, C. M. Burgess, E. D. Cline, S. Bernhard, *Inorg. Chem.* **2009**, *48*, 10498–10506.

[9] P.-Y. Ho, B. Zheng, D. Mark, W.-Y. Wong, D. W. McCamant, R. Eisenberg, *Inorg. Chem.* **2016**, *55*, 8348–8358.

[10] a) G. J. Meyer, *Proc. Natl. Acad. Sci. U. S. A.* **2015**, *112*, 9146–9147; b) B. Zheng, R. P. Sabatini, W.-F. Fu, M.-S. Eum, W. W. Brennessel, L. Wang, D. W. McCamant, R. Eisenberg, *Proc. Natl. Acad. Sci. U. S. A.* **2015**, *112*, E3987–E3996.

[11] a) W. M. Campbell, K. W. Jolley, P. Wagner, K. Wagner, P. J. Walsh, K. C. Gordon, L. Schmidt-Mende, M. K. Nazeeruddin, Q. Wang, M. Grätzel, D. L. Officer, *J. Phys. Chem. C* **2007**, *111*, 11760–11762; b) R. C. Hardison, *Proc. Natl. Acad. Sci. U. S. A.* **1996**, *93*, 5675–5679.

[12] a) M. Gouterman, *J. Mol. Spectrosc.* **1961**, *6*, 138–163; b) T. Hashimoto, Y.-K. Choe, H. Nakano, K. Hirao, *J. Phys. Chem. A* **1999**, *103*, 1894–1904; c) X. Huang, K. Nakanishi, N. Berova, *Chirality* **2000**, *12*, 237–255.

[13] a) C.-W. Lee, H.-P. Lu, C.-M. Lan, Y.-L. Huang, Y.-R. Liang, W.-N. Yen, Y.-C. Liu, Y.-S. Lin, E. W.-G. Diau, C.-Y. Yeh, *Chem. Eur. J.* **2009**, *15*, 1403–1412; b) S.-L. Wu, H.-P. Lu, H.-T. Yu, S.-H. Chuang, C.-L. Chiu, C.-W. Lee, E. W.-G. Diau, C.-Y. Yeh, *Energy Environ. Sci.* **2010**, *3*, 949–955; c) C.-P. Hsieh, H.-P. Lu, C.-L. Chiu, C.-W. Lee, S.-H. Chuang, C.-L. Mai, W.-N. Yen, S.-J. Hsu, E. W.-G. Diau, C.-Y. Yeh, *J. Mater. Chem.* **2010**, *20*, 1127–1134.

[14] a) A. Yella, H.-W. Lee, H. N. Tsao, C. Yi, A. K. Chandiran, M. K. Nazeeruddin, E. W.-G. Diau, C.-Y. Yeh, S. M. Zakeeruddin, M. Grätzel, *Science* **2011**, *334*, 629–634; b) H.-P. Wu, Z.-W. Ou, T.-Y. Pan, C.-M. Lan, W.-K. Huang, H.-W. Lee, N. M. Reddy, C.-T. Chen, W.-S. Chao, C.-Y. Yeh, E. W.-G. Diau, *Energy Environ. Sci.* **2012**, *5*, 9843–9848; c) T. Ripolles-Sanchis, B.-C. Guo, H.-P. Wu, T.-Y. Pan, H.-W. Lee, S. R. Raga, F. Fabregat-Santiago, J. Bisquert, C.-Y. Yeh, E. W.-G. Diau, *Chem. Commun.* **2012**, *48*,

4368–4370; d) M. Urbani, M. Grätzel, M. K. Nazeeruddin, T. Torres, *Chem. Rev.* **2014**, *114*, 12330–12396.

[15] C. Y. Lee, J. T. Hupp, *Langmuir* **2010**, *26*, 3760-3765.

[16] a) A. Burghart, H. Kim, M. B. Welch, L. H. Thoresen, J. Reibenspies, K. Burgess, F. Bergström, L. B. Å. Johansson, *J. Org. Chem.* **1999**, *64*, 7813–7819; b) Y.-C. Liu, H.-H. Chou, F.-Y. Ho, H.-J. Wei, T.-C. Wei, C.-Y. Yeh, *J. Mater. Chem. A* **2016**, *4*, 11878–11887.

[17] J. Karolin, L. B. A. Johansson, L. Strandberg, T. Ny, *J. Am. Chem. Soc.* **1994**, *116*, 7801–7806.

[18] a) M. R. Topka, P. H. Dinolfo, *ACS Appl. Mater. Interfaces* **2015**, *7*, 8053–8060; b) M. T. Whited, P. I. Djurovich, S. T. Roberts, A. C. Durrell, C. W. Schlenker, S. E. Bradforth, M. E. Thompson, *J. Am. Chem. Soc.* **2011**, *133*, 88–96; c) M. J. Leonardi, M. R. Topka, P. H. Dinolfo, *Inorg. Chem.* **2012**, *51*, 13114–13122.

[19] M. Galletta, F. Puntoriero, S. Campagna, C. Chiorboli, M. Quesada, S. Goeb, R. Ziessel, *J. Phys. Chem. A* **2006**, *110*, 4348–4358.

[20] X. Li, J. Yu, J. Low, Y. Fang, J. Xiao, X. Chen, *J. Mater. Chem. A* **2015**, *3*, 2485–2534.

[21] I. Chung, B. Lee, J. He, R. P. H. Chang, M. G. Kanatzidis, *Nature* **2012**, *485*, 486–489.

[22] S. A. Haque, E. Palomares, B. M. Cho, A. N. M. Green, N. Hirata, D. R. Klug, J. R. Durrant, *J. Am. Chem. Soc.* **2005**, *127*, 3456–3462.

[23] T. Bessho, E. Yoneda, J.-H. Yum, M. Guglielmi, I. Tavernelli, H. Imai, U. Rothlisberger, M. K. Nazeeruddin, M. Grätzel, *J. Am. Chem. Soc.* **2009**, *131*, 5930–5934.

[24] a) H. Choi, C. Baik, S. O. Kang, J. Ko, M.-S. Kang, M. K. Nazeeruddin, M. Grätzel, *Angew. Chem. Int. Ed.* **2008**, *47*, 327–330; b) A. Orbelli Biroli, F. Tessore, M. Pizzotti, C.

Biaggi, R. Ugo, S. Caramori, A. Aliprandi, C. A. Bignozzi, F. De Angelis, G. Giorgi, E. Licandro, E. Longhi, *J. Phys. Chem. C* **2011**, *115*, 23170–23182.

[25] M. R. di Nunzio, B. Cohen, S. Pandey, S. Hayse, G. Piani, A. Douhal, *J. Phys. Chem. C* **2014**, *118*, 11365–11376.

[26] M. Shrestha, L. Si, C.-W. Chang, H. He, A. Sykes, C.-Y. Lin, E. W.-G. Diau, *J. Phys. Chem. C* **2012**, *116*, 10451–10460.

[27] C. Qin, A. Mirloup, N. Leclerc, A. Islam, A. El-Shafei, L. Han, R. Ziessel, *Adv. Energy Mater.* **2014**, *4*, 1400085.

[28] a) X. Zhang, T. Peng, L. Yu, R. Li, Q. Li, Z. Li, *ACS Catal.* **2015**, *5*, 504–510; b) X. Zhang, L. Yu, C. Zhuang, T. Peng, R. Li, X. Li, *RSC Adv.* **2013**, *3*, 14363–14370; c) X. Zhang, B. Peng, T. Peng, L. Yu, R. Li, J. Zhang, *J. Power Sources* **2015**, *298*, 30–37.

[29] J. Park, G. Viscardi, C. Barolo, N. Barbero, *Chimia* **2013**, *67*, 129–135.

[30] R. P. Sabatini, B. Zheng, W.-F. Fu, D. J. Mark, M. F. Mark, E. A. Hillenbrand, R. Eisenberg, D. W. McCamant, *J. Phys. Chem. A* **2014**, *118*, 10663–10672.

[31] P. Piatkowski, C. Martin, M. R. di Nunzio, B. Cohen, S. Pandey, S. Hayse, A. Douhal, *J. Phys. Chem. C* **2014**, *118*, 29674–29687.

[32] M. Natali, *ACS Catal.* **2017**, 1330–1339.

[33] a) G. Cerullo, M. Nisoli, S. Stagira, S. De Silvestri, *Opt. Lett.* **1998**, *23*, 1283-1285; b) G. Cerullo, S. D. Silvestri, *Rev. Sci. Instrum.* **2003**, *74*, 1-18.

[34] M. A. L. Marques, E. K. U. Gross, *Annu. Rev. Phys. Chem.* **2004**, *55*, 427–455.

[35] M. J. Frisch, G. W. Trucks, H. B. Schlegel, G. E. Scuseria, M. A. Robb, J. R. Cheeseman, G. Scalmani, V. Barone, B. Mennucci, G. A. Petersson, H. Nakatsuji, M. Caricato, X. Li, H. P. Hratchian, A. F. Izmaylov, J. Bloino, G. Zheng, J. L. Sonnenberg, M. Hada, M.

Ehara, K. Toyota, R. Fukuda, J. Hasegawa, M. Ishida, T. Nakajima, Y. Honda, O. Kitao, H. Nakai, T. Vreven, J. A. Montgomery Jr., J. E. Peralta, F. Ogliaro, M. J. Bearpark, J. Heyd, E. N. Brothers, K. N. Kudin, V. N. Staroverov, R. Kobayashi, J. Normand, K. Raghavachari, A. P. Rendell, J. C. Burant, S. S. Iyengar, J. Tomasi, M. Cossi, N. Rega, N. J. Millam, M. Klene, J. E. Knox, J. B. Cross, V. Bakken, C. Adamo, J. Jaramillo, R. Gomperts, R. E. Stratmann, O. Yazyev, A. J. Austin, R. Cammi, C. Pomelli, J. W. Ochterski, R. L. Martin, K. Morokuma, V. G. Zakrzewski, G. A. Voth, P. Salvador, J. J. Dannenberg, S. Dapprich, A. D. Daniels, Ö. Farkas, J. B. Foresman, J. V. Ortiz, J. Cioslowski, D. J. Fox, Gaussian, Inc., Wallingford CT, **2009**.

[36] a) A. D. Becke, *Phys. Rev. A* **1988**, *38*, 3098–3100; b) C. Lee, W. Yang, R. G. Parr, *Phys. Rev. B* **1988**, *37*, 785–789; c) P. J. Stephens, F. J. Devlin, C. F. Chabalowski, M. J. Frisch, *J. Phys. Chem.* **1994**, *98*, 11623–11627.